Metrol. Meas. Syst., Vol. XIX (2012), No. 1, pp. 29-38.

PAN POLSKA AKADEMIA NAUK

METROLOGY AND MEASUREMENT SYSTEMS

Index 330930, ISSN 0860-8229

www.metrology.pg.gda.pl

M&MS

MATHEMATICAL MODEL OF DYNAMIC WORK CONDITIONS IN THE MEASURING CHAMBER OF AN AIR GAUGE

Czeslaw Janusz Jermak[1)], Andrzej Spyra[2)], Miroslaw Rucki[1)]

1) Poznan University of Technology, Institute of Mechanical Technology, pl. M. Sklodowskiej-Curie 5, 60-965 Poznan, Poland, (✉cz.jermak@interia.pl, miroslaw.rucki@put.poznan.pl)

2) Opole University of Technology, Department of Thermal Engineering and Industrial Facilities, Mikolajczyka 5, 45-271 Opole, Poland, (a.spyra@po.opole.pl)

Abstract

The goal of the proposed computational model was to evaluate the dynamical properties of air gauges in order to exploit them in such industrial applications as in-process control, form deviation measurement, dynamical measurement. The model is based on Reynolds equations complemented by the k-ε turbulence model. The boundary conditions were set in different areas (axis of the chamber, side surfaces, inlet pipeline and outlet cross-section) as Dirichlet's and Neumann's ones. The TDMA method was applied and the efficiency of the calculations was increased due to the "line-by-line" procedure. The proposed model proved to be accurate and useful for non-stationary two-dimensional flow through the air gauge measuring chamber.

Keywords: air gauges, dynamic measurement, in-process control.

1. Introduction

Air gauges are well known precise measuring devices which recently regain scientific interest [1, 2], as well as interest of industrial enterprises [3, 4]. It is crucial to investigate thoroughly the dynamical properties of the air gauges, because they are applied in systems of in-process control (dynamical dimensional measurement) [5, 6], in measuring automatons (quick measurement) [7], in topography measurement (periodic signal) [8], in form deviation measurement [9] and so on. In such conditions, with the input signal changing in time, perfect reproduction of the input signal is not possible and certain dynamic error is inevitable.

To improve dynamical properties of the air gauges, their measuring chamber volumes are substantially reduced down to several cm^3, and the sensing part is based on of piezoresistive pressure transducers built into the measuring chamber [10]. Series of experimental investigations have been performed on the dynamical properties of this kind of air gauges [4, 11, 12].

Measurement science has become closely associated with computer, information, control and systems science [13]. The rapid development of computer science, signal processing, material science etc., enables us to use more precise and more sophisticated methods for data processing that were too complicated to be conducted in the past [14]. The present work deals with the mathematical model of the air flow through a reduced-volume measuring chamber of air gauge in dynamic conditions of measurement (non-stationary state). Based on scientific publications (e.g. [15]), the turbulence model k-ε was chosen as the most appropriate for the investigated case.

Article history: received on May 11, 2011; accepted on Jan. 17, 2012; available online on March 12, 2012.

2. Model of the measuring chamber and the boundary conditions

The scheme of the back-pressure air gauge is presented in Fig. 1 [3]. Its model used for experimental investigation is shown in Fig. 2. Typically, the back-pressure p_k in the measuring chamber represents the dimension-dependent value of the displacement s between the measuring nozzle and the flapper surface. When the outlet orifice of the measuring nozzle is closed by the flapper surface, the pressure in the measuring chamber is equal to the feeding pressure: $p_k = p_z$.

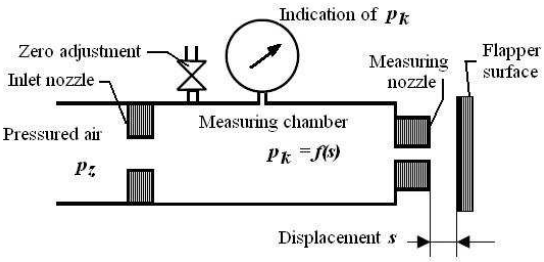

Fig. 1. Scheme of the typical back-pressure air gauge [3].

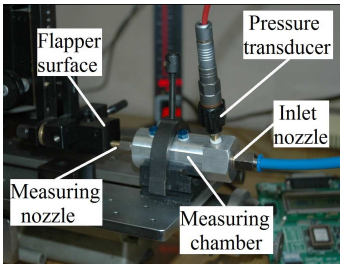

Fig. 2. Experimental setup.

The proposed mathematical model applies the Reynolds equations complemented by the turbulence model k-ε. The equations for nonstationary flow through the air gauge measuring chamber, may be written in general form [16]:

$$\frac{\partial(\rho\Phi)}{\partial t}+\frac{\partial(\rho U\Phi)}{\partial z}+\frac{1}{r}\frac{\partial(\rho rV\Phi)}{\partial r}=\frac{\partial}{\partial z}\left(\Gamma_\Phi\frac{\partial\Phi}{\partial z}\right)+\frac{1}{r}\frac{\partial}{\partial r}\left(r\Gamma_\Phi\frac{\partial\Phi}{\partial r}\right)+S_\Phi, \qquad (1)$$

where: Φ represents subsequently components of the velocity vector (axial U and radial V), kinetic energy of turbulence k and its dissipation velocity ε.

The flow is assumed to be axially-symmetric, and coordinates z and r define the localization of each calculated point. Coefficients Γ_Φ and S_Φ for each variable are presented in Table 1. When it is assumed that $\Phi = \rho$; $\Gamma_\Phi = S_\Phi = 0$, then the equation (1) becomes the equation of flow continuity.

Table 1. Coefficients for the equation (1) [17].

Φ	Γ_Φ	S_Φ
U	μ_{ef}	$\frac{\partial}{\partial z}\left(\mu_{ef}\frac{\partial U}{\partial z}\right)+\frac{1}{r}\frac{\partial}{\partial r}\left(r\mu_{ef}\frac{\partial V}{\partial z}\right)-\frac{\partial p}{\partial z}$
V	μ_{ef}	$\frac{\partial}{\partial z}\left(\mu_{ef}\frac{\partial U}{\partial r}\right)+\frac{1}{r}\frac{\partial}{\partial r}\left(r\mu_{ef}\frac{\partial V}{\partial r}\right)-\frac{\partial p}{\partial r}-\mu_{ef}\frac{V}{r^2}$
k	$\frac{\mu_{ef}}{\sigma_k}$	$G-\rho\varepsilon$
ε	$\frac{\mu_{ef}}{\sigma_\varepsilon}$	$\frac{\varepsilon}{k}\left(C_1G-C_2\rho\varepsilon\right)$

where: $G=\mu_t\left\{2\left[\left(\frac{\partial U}{\partial z}\right)^2+\left(\frac{\partial V}{\partial r}\right)^2\right]+\left(\frac{V}{r^2}\right)+\left(\frac{\partial U}{\partial r}+\frac{\partial V}{\partial z}\right)^2\right\}$; $\mu_{ef}=\mu+\mu_t$; $\quad \mu_t=C_\mu\rho\frac{k^2}{\varepsilon}$.

The values C_μ, C_1, C_2, σ_k and σ_ε are the constants of the turbulence model. According to [18], their values may be assumed as it is shown in Table 2.

Table 2. Constants of the turbulence model.

C_μ	C_1	C_2	σ_k	σ_ε
0.09	1.44	1.92	1.0	1.3

Those constants presented in Table 2 have been determined experimentally. They provide accurate results of calculations for most cases.

In Fig. 3, the computational domain inside the air gauge measuring chamber of length l_k and diameter d_k is presented. Values l_d and d_w correspond with the length and diameter of inlet nozzle, respectively. Because of assumed flow symmetry, the axis may set the bound γ_2, the side surfaces of the inlet nozzle and the measuring chamber set the bounds γ_3, and the cross-sections of inlet pipeline γ_1 and measuring nozzle γ_4 set the rest of the boundaries.

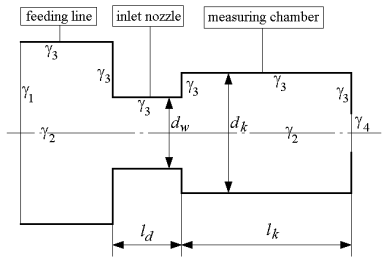

Fig. 3. The computational domain inside the air gauge measuring chamber.

The way of setting of boundary conditions for equation (1) is dependent on the specific solved problem. In the actual research, it was assumed that at the moment $t = 0$, all the system (inlet pipe – inlet nozzle – measuring chamber) remains in the initial state of rest ($U = V = 0$), and its pressure $p_k = p_z = 0.15$ MPa. Such conditions take place when the measuring nozzle is closed by the flapper surface. In the time $t > 0$, the measuring slot goes wider and the air flows outside, causing changes in back-pressure $p_k = f(s)$.

In the inlet cross section γ_1, all variables must fulfill Dirichlet's condition:

$$\Phi\Big|_{\gamma_1} = \Phi(r), \tag{2}$$

where: Φ represents subsequently components of the velocity vector U and V, kinetic energy of turbulence k and its dissipation velocity ε.

In the symmetry axis of the measuring chamber $V = 0$, for the variables $\Phi = U, k, \varepsilon$ the Neumann's boundary condition was assumed:

$$\frac{\partial \Phi}{\partial r}\Big|_{\gamma_2} = 0. \tag{3}$$

In the outlet intersection γ_4, all variables kept the Neumann's condition:

$$\frac{\partial \Phi}{\partial z}\Big|_{\gamma_4} = 0. \tag{4}$$

For the inner surfaces of the measuring chamber and the inlet nozzle, boundary conditions were set according to the assumption of non-sliding and non-penetrable movement of the air stream along the surfaces:

$$U\Big|_{\gamma 3} = 0; V\Big|_{\gamma 3} = 0. \tag{5}$$

It was derived from the "logarithmic law of the wall" which is applied along with the k~ε model for the developed turbulence.

3. Digital approximation of the differential equations of the model

Approximation of the equation, as well as the applied algorithm were based on the work [17]. Some modifications in respect of the dynamic conditions were introduced and the continuous area of the measuring chamber was replaced with the discrete non-uniform grid (Fig. 4).

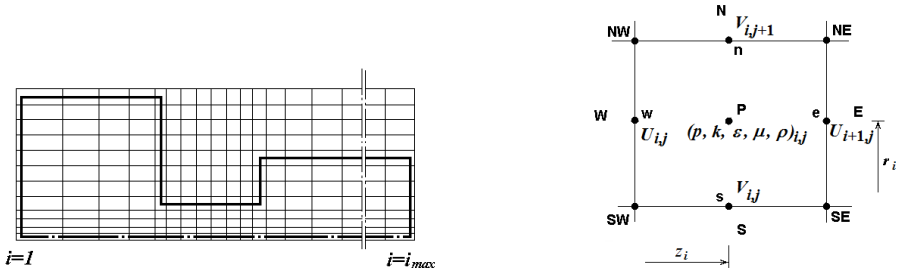

Fig. 4. Discretization of the calculation area.

When both sides of the equation (1) are multiplied by r, the resulting formula is particularly easy to be approximated differentially:

$$r\frac{\partial(\rho\Phi)}{\partial t} + \frac{\partial(\rho r U\Phi)}{\partial z} + \frac{\partial(\rho r V\Phi)}{\partial r} = \frac{\partial}{\partial z}\left(r\Gamma_\Phi \frac{\partial\Phi}{\partial z}\right) + \frac{\partial}{\partial r}\left(r\Gamma_\Phi \frac{\partial\Phi}{\partial r}\right) + rS_\Phi. \tag{6}$$

Equations for each variable are quite similar, therefore the following is presented for the general variable Φ, and the differences are discussed:

The first term of the equation (6) is approximated as follows:

$$r\frac{\partial(\rho\Phi)}{\partial t} \approx r_j \frac{\Phi_{i,j}^{(n+1)} - \Phi_{i,j}^{(n)}}{\Delta t}, \tag{7}$$

which may be rewritten as:

$$r\frac{\partial(\rho\Phi)}{\partial t} \approx M_P(\rho\Phi)_{i,j}^{(n+1)} - M_P(\rho\Phi)_{i,j}^{(n)}, \tag{8}$$

where: $M_P = \dfrac{r_j}{\Delta t}$, while indexes and n, $n+1$ correspond with subsequent values of time t.

Diffusional terms of the equation (6) are approximated as following:

$$\frac{\partial}{\partial z}\left(r\Gamma_\Phi \frac{\partial\Phi}{\partial z}\right) \approx \frac{1}{\overline{\Delta z_i}}\left[\left(r\Gamma_\Phi\right)_{i+1/2,j} \frac{\Phi_{i+1,j} - \Phi_{i,j}}{\Delta z_{i+1}} - \left(r\Gamma_\Phi\right)_{i-1/2,j} \frac{\Phi_{i,j} - \Phi_{i-1,j}}{\Delta z_i}\right], \tag{9}$$

$$\frac{\partial}{\partial r}\left(r\Gamma_\Phi \frac{\partial\Phi}{\partial r}\right) \approx \frac{1}{\overline{\Delta r_j}}\left[\left(r\Gamma_\Phi\right)_{i,j+1/2} \frac{\Phi_{i,j+1} - \Phi_{i,j}}{\Delta r_{j+1}} - \left(r\Gamma_\Phi\right)_{i,j-1/2} \frac{\Phi_{i,j} - \Phi_{i,j-1}}{\Delta r_j}\right], \tag{10}$$

where:

$$\Delta z_i = z_i - z_{i-1}; \Delta z_{i+1} = z_{i+1} - z_i; \quad \Delta r_j = r_j - r_{j-1}; \Delta r_{j+1} = r_{j+1} - r_j; \quad \overline{\Delta z}_i = \frac{\Delta z_i + \Delta z_{i+1}}{2}; \quad \overline{\Delta r}_j = \frac{\Delta r_j + \Delta r_{j+1}}{2}.$$

After transformations, the share of diffusional terms may be approximated as follows:

$$\frac{\partial}{\partial z}\left(r\Gamma_\Phi \frac{\partial \Phi}{\partial z}\right) + \frac{\partial}{\partial r}\left(r\Gamma_\Phi \frac{\partial \Phi}{\partial r}\right) \approx D_E\Phi_E + D_W\Phi_W + D_N\Phi_N + D_S\Phi_S - D_P\Phi_P, \tag{11}$$

where:

$$D_E = \frac{\left(r_j \mathrm{G_F}\right)_e}{\mathrm{D}z_i \mathrm{D}z_{i+1}}; D_N = \frac{\left(r_{j+1/2} \mathrm{G_F}\right)_n}{\overline{\mathrm{D}r}_j \mathrm{D}r_{j+1}}; D_W = \frac{\left(r_j \mathrm{G_F}\right)_w}{\mathrm{D}z_i \mathrm{D}z_i}; D_S = \frac{\left(r_{j-1/2} \mathrm{G_F}\right)_s}{\overline{\mathrm{D}r}_j \mathrm{D}r_j}; D_P = D_E + D_W + D_N + D_S.$$

Convectional terms of the equation (6) are approximated with the central differences:

$$\frac{\partial\left(r\rho U\Phi\right)}{\partial z} \approx \frac{r_j}{\overline{\Delta z}_i}\left[U_{i+1,j}\frac{(\rho\Phi)_{i+1,j} + (\rho\Phi)_{i,j}}{2} - U_{i,j}\frac{(\rho\Phi)_{i,j} + (\rho\Phi)_{i-1,j}}{2}\right], \tag{12}$$

$$\frac{\partial\left(r\rho U\Phi\right)}{\partial r} \approx \frac{1}{\overline{\Delta r}_j}\left[r_{j+1/2}V_{i,j+1}\frac{(\rho\Phi)_{i,j+1} + (\rho\Phi)_{i,j}}{2} - r_{j-1/2}V_{i,j}\frac{(\rho\Phi)_{i,j} + (\rho\Phi)_{i,j-1}}{2}\right]. \tag{13}$$

After transformations, the share of convectional terms may be approximated as follows:

$$\frac{\partial\left(r\rho U\Phi\right)}{\partial z} + \frac{\partial\left(r\rho U\Phi\right)}{\partial r} \approx C_E\Phi_E - C_W\Phi_W + C_N\Phi_N - C_S\Phi_S + C_P\Phi_P, \tag{14}$$

where:

$$C_E = \frac{r_j U_{i+1,j}}{2\overline{\mathrm{D}z}_i}; C_N = \frac{r_{j+1/2}V_{i,j+1}}{2\overline{\mathrm{D}r}_j}; C_W = \frac{r_j U_{i,j}}{2\overline{\mathrm{D}z}_i}; C_S = \frac{r_{j-1/2}V_{i,j}}{2\overline{\mathrm{D}r}_j}; C_P = C_E - C_W + C_N - C_S.$$

To ensure a stable difference scheme, the summed share of the convectional and diffusional terms is calculated according to the hybrid scheme [19]:

$$\begin{aligned} &A_N = \max\{D_N, |C_N|\} - C_N; A_S = \max\{D_S, |C_S|\} + C_S; \\ &A_E = \max\{D_E, |C_E|\} - C_E; A_W = \max\{D_W, |C_W|\} + C_W; \\ &A_P = A_N + A_S + A_E + A_W. \end{aligned} \tag{15}$$

The source term of the equation (6) is linearized to the form:

$$S_\mathrm{F} = S_P^\mathrm{F} + S_U^\mathrm{F}, \tag{16}$$

where: S_P^Φ, S_U^Φ are the coefficients dependent on the type of variables. They are calculated according to the formulas described in [17]. The partial derivatives present in the formulas of S^Φ, are approximated using the scheme of "central difference".

After the differential approximation of the equation (6), the obtained formulas may be joined together to the following function:

$$a_P^\Phi\Phi_P = a_E^\Phi\Phi_E + a_W^\Phi\Phi_W + a_N^\Phi\Phi_N + a_S^\Phi\Phi_S + r_j S_U^\Phi + M_P\Phi_P^{(n)}, \tag{17}$$

where: $a_P^\Phi = a_E^\Phi + a_W^\Phi + a_N^\Phi + a_S^\Phi - r_j S_P^\Phi + M_P$.

All the values of the variables in the equation (17) are calculated for the $n + 1$ time level, except of the term $M_P \Phi_P^{(n)}$. This one is calculated on the basis of the value taken from the "old" (n) time level. The coefficients a^Φ for each variable are as follows:

$$a_E^\Phi = A_E; a_W^\Phi = A_W; a_N^\Phi = A_N; a_S^\Phi = A_S.$$

4. Discretized equations of non-stationary state in measuring chamber

In the differential equation (17), every value of the function Φ in point P is dependent on the values in four neighboring points E, W, N, S (Fig. 4). Equations for the velocity vector components U and V are transformed in a similar way as the equation (17). However, two important differences should be marked. First, differential approximation is made in the grid, where the values of $U_{i,j}$ or $V_{i,j}$ are placed in the central points. And secondly, the source terms for both components S_U^U, S_U^V contain additionally pressure differences between two neighboring cells. This difference is the result of approximation of derivatives $\frac{\partial p}{\partial z}$ and $\frac{\partial p}{\partial r}$.

The differential equation for the component U may be written as the following formula:

$$a_P^U U_P = a_E^U U_E + a_W^U U_W + a_N^U U_N + a_S^U U_S + r_{j-1/2} S_U^{U*} + r_j \frac{p_w - p_P}{\Delta z_i} + M_P \Phi_P^{(n)} \tag{18}$$

and for the component V:

$$a_P^V U_P = a_E^V U_E + a_W^V U_W + a_N^V U_N + a_S^V U_S + r_{j-1/2} S_U^{V*} + r_{j-1/2} \frac{p_s - p_P}{\Delta r_j} + M_P \Phi_P^{(n)}. \tag{19}$$

The coefficients a_P^V, a_U^V are calculated in the same way as for the equation (17), and the values S_U^{U*}, S_U^{V*} mean the discretized approximation of the other than pressure components: S_U^U, S_U^V. However, the exact values of the pressure p in the grid joints are not known in the moment when the equations (18) and (19) are solved, therefore the approximate value p^* is taken instead, typically from the previous time level or from the last iteration. As a result, from the formulas (18) and (19) approximate values V^* and U^* are obtained in all the grid joints. The exact value of the pressure p is calculated from the formula:

$$p = p^* + p', \tag{20}$$

where: p' is the pressure correction calculated from the separate equation. The exact values of the velocity, which meet the requirement of flow continuity, may be calculated as follows:

$$\begin{aligned} U_P &= U_P^* + D^U(p'_W - p'_P), \\ V_P &= V_P^* + D^V(p'_S - p'_P), \end{aligned} \tag{21}$$

where: $D^U = \frac{1}{\Delta z_i a_P^U}; D^V = \frac{1}{\Delta r_j a_P^V}$.

It is necessary to calculate the pressure correction p' in each grid joint to ensure the conformity of calculated values U and V with the flow continuity equation:

$$\frac{\partial p}{\partial t} + \frac{\partial(\rho U)}{\partial z} + \frac{1}{r}\frac{\partial(r\rho V)}{\partial r} = 0. \tag{22}$$

To obtain the discretized form of the equation (22), the formulas (21) should be put in. It leads to the following formula:

$$r_j \frac{\rho_{i,j}^{(n+1)} - \rho_{i,j}^{(n)}}{\Delta t} + \frac{r_j}{\Delta z_i}\left(U_{i+1,j} - U_{i,j}\right) + \frac{1}{\Delta r_j}\left(r_{j+1/2}V_{i,j+1} - r_{j-1/2}V_{i,j}\right) = 0. \tag{23}$$

The equations (21) may be rewritten as follows:

$$\begin{aligned} U_{i,j} &= U_{i,j}^* + \frac{p'_W - p'_P}{\mathrm{D}z_i a_P^U}; U_{i+1,j} = U_{i+1,j}^* + \frac{p'_P - p'_E}{\mathrm{D}z_{i+1} a_P^U}, \\ V_{i,j} &= V_{i,j}^* + \frac{p'_S - p'_P}{\mathrm{D}r_j a_P^V}; V_{i,j+1} = V_{i,j+1}^* + \frac{p'_P - p'_N}{\mathrm{D}r_{j+1} a_P^V}. \end{aligned} \tag{24}$$

Then Poisson's equation for the pressure correction may be obtained:

$$a_P^P p' = a_E^P U_E + a_W^P p'_W + a_N^P p'_N + a_S^P p'_S + S_U^P, \tag{25}$$

where:

$$a_E^P = \frac{r_j}{\Delta z_i \Delta z_{i+1} a_P^U}; a_W^P = \frac{r_j}{\Delta z_i \Delta z_i a_P^U}; a_N^P = \frac{r_{j+1/2}}{\Delta r_j \Delta r_{j+1} a_P^V}; a_S^P = \frac{r_{j-1/2}}{\Delta r_j \Delta r_j a_P^V},$$

$$S_U^P = \frac{r_j}{\Delta z_i}\left(U_{i,j}^* - U_{i+1,j}^*\right) + \frac{1}{\Delta r_j}\left(r_{j-1/2}V_{i,j}^* - r_{j+1/2}V_{i,j+1}^*\right).$$

To obtain the discretized boundary conditions, the differential grid was used. In the discretized form, the bound γ_1 must fulfill the Dirichlet's condition for all variables:

$$\Phi_{1,j} = \Phi_0(r). \tag{26}$$

In the points next to the side surfaces, the boundary conditions are based on the "logarithmic law of the wall". Following is the example concerning the side parallel to the *z*-axis. Here, the values of the velocity in the point next to the side surface is marked with index *sc*.

The kinetic energy of turbulence k_{sc} is calculated from the general equation (17), while the convection is neglected. The diffusion in the direction normal the side surface is considered to be zero: $a_N^k = 0$. The source term of the equation is simplified:

$$S_U^k = \left|\tau_w \frac{\partial U}{\partial r}\right|, \tag{27a}$$

$$S_P^k = -C_\mu k^{1/2} \frac{\ln(En^+)}{\kappa \Delta n}, \tag{27b}$$

where: $\tau_w = \frac{C_\mu k^{1/2} \kappa}{\ln(En^+)} U_{sc}$ - tangent stress on the side surface, κ, E - are the experimentally determined constants (κ = 0.42; E = 9.7), $n^+ = k^{1/2} C_\mu^{1/4} \Delta n / V$ - dimensionless distance from the side surface, Δn – the above distance with dimension.

The value of kinetic turbulence energy dissipation in the point next to the side surface, is calculated from the following formula:

$$\varepsilon_{sc} = \frac{C_\mu^{3/4} k^{3/2}}{\kappa \Delta n}. \tag{28}$$

In the symmetry axis, the boundary condition for the variable V is of Dirichlet type:

$$V_{i,1} = 0 \tag{29}$$

and for the rest of variables, of Neumann type:

$$\Phi_{i,1} = \Phi_{i,2}\,. \tag{30}$$

In the outlet cross-section, all the variables Φ have got the Neumann's boundary condition in the following form:

$$\Phi_{i\max,j} = \Phi_{i\max-1,j}\,. \tag{31}$$

5. Iteration solution of the discretized equations

Fig. 5 presents the block diagram of the calculation algorithm.

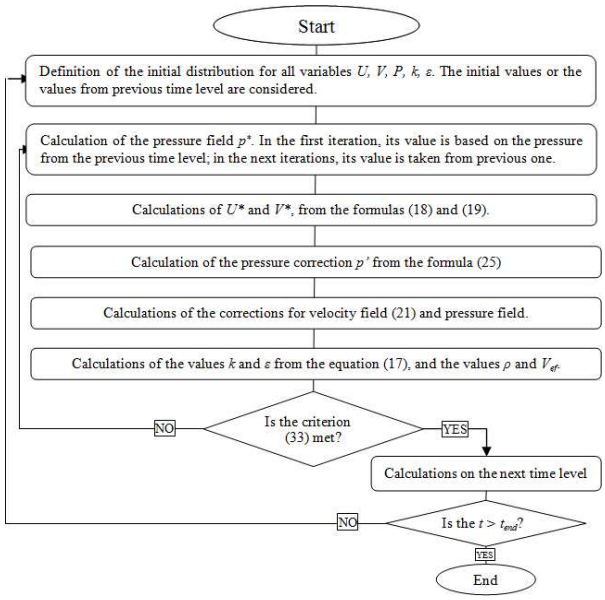

Fig. 5. The iteration algorithm.

In each time level, iteration should be performed in order to solve the system of differential equations for every variable Φ. The efficiency of the calculations was increased due to the procedure "line-by-line". To perform it, the differential equation (17) was transformed into the formula:

$$-a_N^{\Phi}\Phi_N + a_P^{\Phi}\Phi_P - a_S^{\Phi}\Phi_S = F_{\Phi}\,, \tag{32}$$

where: $F_{\Phi} = a_E^{\Phi}\Phi_E + a_W^{\Phi}\Phi_W + r_j S_U^{\Phi} + M_P\Phi_P^{(n)}$.

The equation (32) is solved simultaneously in the whole grid line using the TDMA method [19]. For each variable, the iteration cycle is repeated several times (2 to 5 times). The convergence criterion of the iteration process is the condition:

$$\max_{\Phi}\left\{\mathrm{Res}\,(\Phi)\right\} \le \lambda\,, \tag{33}$$

where: $\mathrm{Res}(\Phi) = \max_{i,j}\left\{a_P^{\Phi}\Phi_p - \sum_{N,S,E,W} a_j^{\Phi}\Phi_j - S_U^{\Phi}\right\}$.

The residual criterion above (33) is the necessary condition of the convergence of iteration process. It postulates with certain accuracy λ that the differential equations are fulfilled in all points of the grid for each variable Φ.

6. The simulation results

The simulations were performed for a cylindrical inlet nozzle of length l_d = 6.06 mm and diameter d_w = 2.025 mm leading into the measuring chamber of diameter 10 mm and length 40 mm. The inlet pipe diameter was 15 mm with assumed steady velocity distribution $U(r) = U_0$. The feeding pressure p_z = 0.15 MPa, barometric pressure p_a = 0.101325 MPa. The air density was calculated for the temperature T = 293 K, and mass flow 6×10^{-4} kg/s. The time was assumed from 0.001 s to 0.11 s with step Δt = 0.001 s.

The simulations provided the information on the flow through the air gauge measuring chamber. Fig. 6 presents the obtained profiles of the velocity component U in several cross-sections, and the Fig. 7 provides the chart of the values of velocity vectors and their directions.

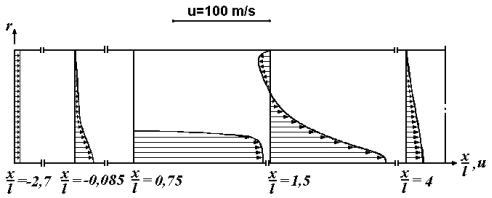

Fig. 6. The velocity profiles inside the air gauge measuring chamber.

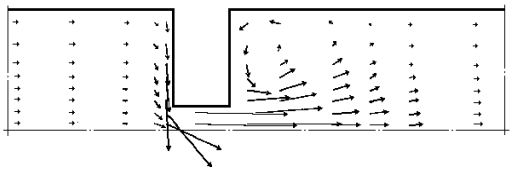

Fig. 7. The velocity vectors inside the air gauge measuring chamber.

7. Conclusions

The proposed mathematical model for nonstationary flow through the air gauge measuring chamber is based on the Reynolds equations and the k-ε turbulence model. It is useful in the calculations of the nonstationary state of the flow in the measuring chamber of an air gauge, and has been successfully used for the simulation of the flow through the constriction flow meter [20]. It appears from performed comparison of different turbulence models [21] that when simulating a two-dimensional flow through a pipe with constriction, the traditional Launder-Spalding k-ε model yields the best results and involves the lowest calculation cost.

The model applies a set of differential equations, containing the axial and radial components of velocity U and V, the kinetic energy of turbulence k and its dissipation velocity ε. The flow is assumed to be axi-symmetrical, and coordinates z and r define the localization of each point of the calculation area. The discretization grid is non-uniform in order to calculate more accurately the most important areas.

The boundary conditions were set in different areas (axis of the chamber, side surfaces, inlet pipeline and outlet cross-section) as the Dirichlet and Neumann ones. The TDMA method was applied and the efficiency of the calculations was increased due to the "line-by-line" procedure The proposed model proved to be accurate and useful for nonstationary flow through the air gauge measuring chamber.

Acknowledgements

This work was supported by the Ministry of Science and Higher Education, Poland.

References

[1] Hennessy, R. (2005). Use air to improve measurements; manufacturers turn to air gaging for high-resolution measurements. *Quality Magazine,* 30-33.

[2] Zelczak, A. (2002). *Pneumatic dimensional measurements*. Communication Publishing and Communications, Warsaw. (in Polish)

[3] Rucki, M., Barisic, B., Varga, G. (2010). Air gauges as a part of the dimensional inspection systems. *Measurement*, 43(1), 83-91.

[4] Jermak, Cz.J., Rucki, M. (2009). Evaluation of the response time of air gauges in industrial applications. *Metrology and Measurement Systems*, 16(4), 689-700.

[5] Yandayan, T., Burdekin, M. (1997). In-process dimensional measurement and control of workpiece accuracy. *International Journal of Machine Tools and Manufacture*, 37(10), 1423-1439.

[6] Menzies, I., Koshy, P. (2009). In-process detection of surface porosity in machined castings. *International Journal of Machine Tools & Manufacture*, 49, 530-535.

[7] Wang, Y.H., et al. (2005). An Automatic Sorting System Based on Pneumatic Measurement. *Key Engineering Materials*, 295-296, 563-568.

[8] Koshy, P., Grandy, D., Klocke, F. (2011). Pneumatic non-contact topography characterization of finish-ground surfaces using multivariate projection methods. *Precision Engineering,* 35, 282-288.

[9] Jermak, Cz.J., Cellary, A., Rucki M. (2010). Novel method of non-contact out-of-roundness measurement with air gauges. *Proceedings of the Euspen 10th International Conference*, Delft, Holland, 71-74.

[10] Rucki, M., Barisic, B. (2009). Response Time Of Air Gauges with Different Volumes of the Measuring Chambers. *Metrology and Measurement Systems,* 16(2), 289-298.

[11] Rucki, M. (2007). Step Response of the Air Gauge. *Metrology and Measurement Systems,* 14(3), 429-436.

[12] Rucki, M., Barisic, B., Ocenasova, L. (2010). Dynamic calibration of air gauges. *Archives of Mechanical Technology and Automation,* 30(2), 129-134.

[13] Finkelstein, L. (2007). Reflections on a century of measurement science as an academic discipline. *Metrology and Measurement Systems,* 14(4), 635-638.

[14] Janiczek, T., Janiczek, J. (2010). Linear dynamic system identification in the frequency domain using fractional derivatives. *Metrology and Measurement Systems,* 17(2), 279-288.

[15] Woelke, M. (2007). Eddy Viscosity Turbulence Models employed by Computational Fluid Dynamic. *Transactions of the Institute of Aviation*, *Scientific Quarterly*, (4), 191.

[16] Dobrowolski, B., Kabza, Z., Spyra, A. (1988). Digital Simulation of Air Flow Through a Nozzle of Pneumatic Gauge. *Proceedings of 33rd JUREMA Annual Gathering*, Zagreb, 67-70.

[17] *Theory and Practice of Air Gauging* (2011), Monography, ed. Cz.J. Jermak, TU Poznan.

[18] Lauder, B.E., Spalding, D.B. (1974). The Numerical Computation of Turbulent Flows. *Computer Methods in Applied Mechanics and Engineering*, (3), 269-289.

[19] Patankar, S. (1980). *Numerical heat transfer and fluid flow*. New York, Hemisphere.

[20] Dobrowolski, B., Kabza, Z. (1992). Theoretical analysis of the axial symmetric deformation of the velocity field and stream turbulences influences on the metrological properties of the measuring nozzles. *Studies and Monographies*, (59), College of Engineering in Opole. (in Polish)

[21] Dobrowolski, B., Kręcisz, K., Spyra, A. (2005). Usability of selected turbulence models for simulation flow through a pipe orifice. *Task Quarterly,* 9(4), 439-448.